Stress patterns, failure modes, and bone remodeling

Non-Cemented Total Hip Arthroplasty,
edited by R. Fitzgerald, Jr.
Raven Press, Ltd., New York © 1988.

Chapter 24

Stress Patterns, Failure Modes, and Bone Remodeling

R. Huiskes

Biomechanics Laboratory, Department of Orthopaedics, University of Nijmegen, The Netherlands

The problem of failure modes in THA (total hip arthroplasty) is a multifactorial one, involving complex biological and mechanical aspects. Nevertheless, in this chapter we will limit ourselves to the mechanical point of view, and for that purpose a few terms must be defined. It must be appreciated first that clinical failure and mechanical failure are not synonymous. A crack in acrylic cement can be recognized as a mechanical failure but does not necessarily mean that the implant should be revised immediately, if ever.

The primary function of an implant-fixation configuration is to transfer the joint load to the bone through the prosthesis and the fixation material in such a way that the stress patterns accompanying this load-transfer mechanism do not cause failure for the longest possible period of time. The key factor in this function is the implant–bone interface. This interface is an extensive region and should not be considered as an entity. It is either bonded, loose, or a combination of both. "Mechanical interface loosening," therefore, should be defined relative to a specific, local interface region, as the inability of the implant–bone connection to transfer tensile and shear stresses (other than friction). A consequence of a mechanically loose interface region is that local separation and slip [relative (micro) motion] can occur. Local mechanical loosening may propagate to mechanical loosening at large, enhancing the formation of fibrous tissue interposition, visible on x-rays. This process is commonly termed roentgenological loosening, which gradually may develop to clinical loosening, whereby the implant must be revised for reasons of pain and/or function limitation. It is often found that the femoral component of THA is not easily removed during revision surgery, although the diagnoses of roentgenological and clinical loosening have been clearly established. In that case, the prosthesis is jammed in the medullar canal and removal is resisted by friction or local geometrical restrictions. Hence, this phenomenon does not contradict the definition of a mechanically loose interface. In fact, where cement interlocking does not occur or, as to that, bone ingrowth in cementless prostheses does not occur, the interface is mechanically loose, according to the definition, even if the implant is clinically stable.

The primary mechanical problem is now illustrated in Fig. 24.1. The joint load is transferred to the bone, generating stresses in the different materials and at their connections. The stress patterns depend on (a) the magnitude and orientation of the applied load, (b) the geometric configuration, (c) the mechanical properties of the materials (i.e., elastic constants), and (d) the boundary and interface conditions. If, locally, a stress value exceeds the strength

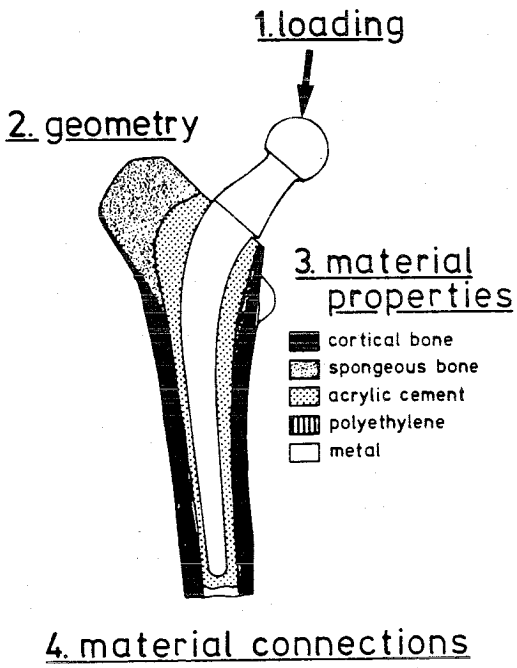

FIG. 24.1. The stress patterns associated with the load-transfer mechanism from prosthesis to bone depend on four aspects.

of a material or a connection, mechanical failure is initiated. Hence, the chances for mechanical failure can be decreased by reducing stresses and/or increasing strength. This is illustrated in Fig. 24.2, relative to chances for implant–bone interface failure. Both the actual interface stress and the interface strength in a patient series will be distributed according to some sort of stochastic function. Where these overlap, mechanical interface failure occurs. Evidently, the chances for failure in a particular hip-joint design are minimal in the case of a maximal average safety margin (asm). Whereas interface strength is a matter of fixation technique and the integrity of the bone interlock, as it depends on biological bone–interface reactions over time, this chapter discusses interface stresses, in particular the relationship between interface stress patterns and implant design.

Eminently suited to evaluate stress patterns in complex structures such as THA configurations, at least in principle, is the finite-element method (FEM) (1,2). This method has

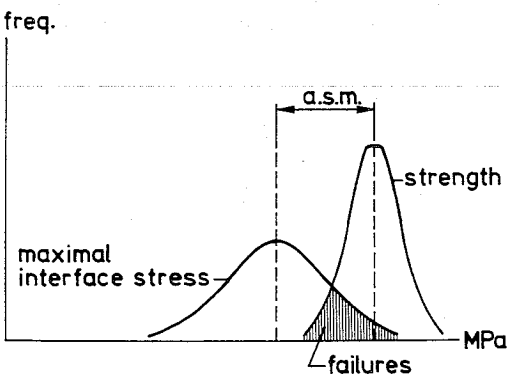

FIG. 24.2. A hypothetical, stochastic model to relate interface stress and strength to the chances for mechanical failure in a patient population (asm = average safety margin).

been used in several investigations to analyze THA designs, which has led to a better general understanding of THA fixation mechanics (3). A second objective of this chapter is to describe some recent advances in the capabilities of the FEM in this respect.

LOAD TRANSFER IN THE PROXIMAL FEMUR

The implant-to-bone load-transfer mechanism in an intramedullary stem fixation, such as the femoral hip component, has some basic characteristics, regardless of the stem shape and the precise joint load. These basic characteristics can be illustrated by a simplified model describing a straight stem cemented in a straight bone tube (4). Fig. 24.3 shows the loads carried by the stem and by the bone and the pattern of the load transferred from the stem to the bone through the cement layer and the interfaces. The first characteristic feature of these internal loading patterns is the load-transfer concentration at the proximal and distal sides, generating stress peaks in the cement and at the interfaces. The second characteristic feature is the "stress shielding" effect in bone, caused by load sharing between stem and bone: the load, carried by the stem at the proximal side, is transferred to the bone in two steps. This load would normally be carried by the bone alone, hence the stress shielding effect.

Although the stress patterns can vastly differ, depending on the joint load and the actual shape of the stem, these basic characteristics of the load-transfer mechanism have been

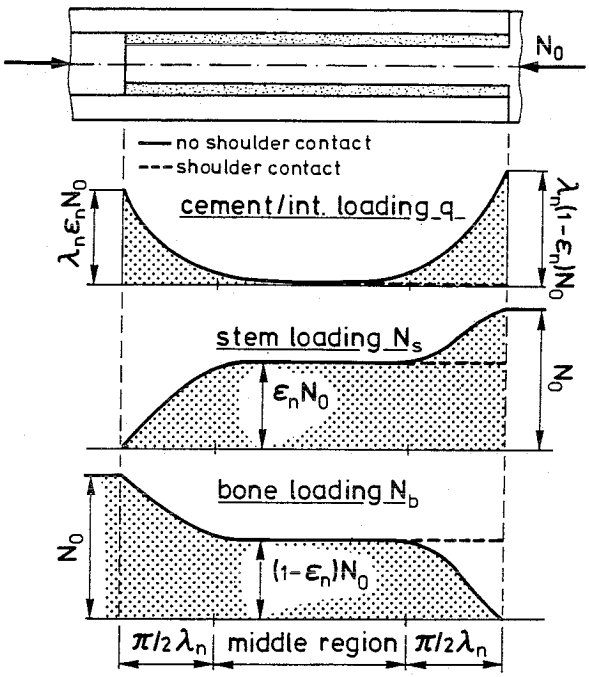

FIG. 24.3. Principles of the load-transfer mechanism explained with a simplified intramedullary fixation model (4), loaded with an axial force N_0. Characteristic features are the load transfer in two steps, proximally and distally, associated with stress peaks in the cement and at the interfaces. Load sharing leads to "stress shielding" of the bone by the stem.

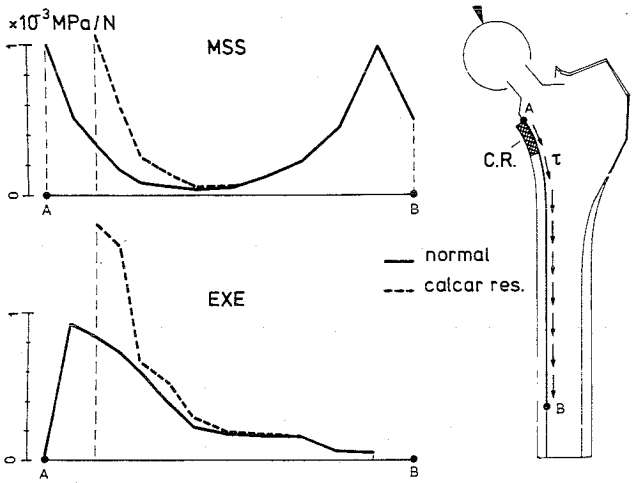

FIG. 24.4. Shear stresses along the medial implant–bone interface, as determined for the Müller straight stem and the Exeter prosthesis (15). Also shown are the shear stresses for the case that 20 mm calcar resorption has occurred.

found in virtually all FEM (5–10) and strain-gauge (11–14) analyses of the femoral THA, and they are adequately supported by basic mechanical considerations (4).

The amount of stress shielding depends mainly on the stiffness (thickness and elastic modulus) of the stem, and the load-transfer stress concentrations depend on the stiffness, the stem taper, and the cement-layer thickness distribution. Fig. 24.4 shows implant–bone interface shear stresses at the medial side, comparing a relatively stiff, straight stem prosthesis (MSS: Müller straight stem) to a more flexible tapered one (EXE: Exeter prosthesis) (15). Evidently, in the latter case the distal stress transfer has diminished owing to the taper shape, which brings about other problems, to be discussed later.

The results, shown in Fig. 24.4, are based on a two-dimensional (2-D) FEM model (16), whereby it is assumed that the structure is symmetric relative to the midfrontal plane, and the load works in that same plane. The three-dimensional (3-D) structural integrity of the structure is taken into account by using a side-plate element layer and a nonuniform element thickness distribution, as illustrated in Fig. 24.5. Hence, the model actually consists of two 2-D models superimposed. In this way the stress patterns are quite adequately represented, with the exception of hoop stresses, provided that the above conditions are met. In reality, the structure is not symmetric and loads do work out of the midfrontal plane. These conditions can be studied with true 3-D FEM models. An example of results is shown in Fig. 24.6, relative to a 3-D FEM model of an experimental cementless prosthesis (10). The basic characteristics of the load-transfer mechanism, as previously discussed, are found here, too. However, the actual stress concentrations per cross section tend to be somewhat off the midfrontal plane, depending on the cross-sectional geometry of the bone, in particular the thickness distribution of the cancellous bone (a cement layer would, qualitatively speaking, have the same effect). As evident in Fig. 24.6, the out-of-plane force component has a significant effect on the magnitudes of the maximal stress values, but less so on their location, very much comparable to the effects of a force rotated toward lateral. This indicates that the bending effect of the hip-joint load in particular is of importance, relative to chances for interface disruption. This point has been stressed before (2,4,6),

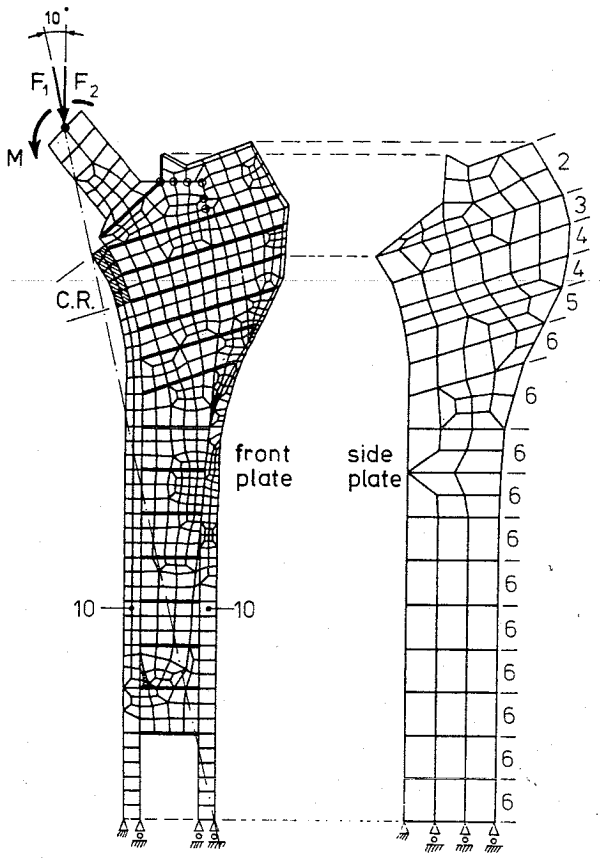

FIG. 24.5. Standardized 2-D FEM model used for comparative stem design testing (16). The model features side-plate and nonuniform thickness distributions to account for the 3-D structural integrity.

and is once more illustrated in Fig. 24.7, where medial and lateral implant–bone interface stresses in a short cementless prosthesis are compared for different joint loads of equal magnitudes (2-D side-plate FEM model) (10). The interface stresses are higher, depending on the amount of bending generated by the force.

A final word must be devoted in this section to implant material. Generally speaking, the more flexible the stem, the more load will be transferred proximally and the less distally (4). It must be appreciated in this respect that the stem diameter has far more effect on stem flexibility than the stem modulus. There is a general feeling that the ideal implant material would be one that mimics the bone elastic properties as closely as possible, because in that case the bone stresses would be close to normal. Although this is true, there is a catch to this solution, related to load transfer. A flexible stem, in particular one made out of a very flexible, hypothetical "isoelastic" material, generates exceptionally high implant–bone interface stresses (shear, tension/compression), in particular at the proximal side. This effect is illustrated in Fig. 24.8, relative to the same cementless prosthesis model as discussed before (Fig. 24.7). Because there must always be an implant–bone interface, the isoelastic solution can work only when a method of fixation can be found whereby the implant–bone connection is reproducibly as strong as bone itself and remains so during the full postoperative period. The question of implant-material flexibility is very much interrelated with implant design and cannot be answered conclusively for all implants in general. Where intramedullary stem fixation is concerned, the use of stiff materials,

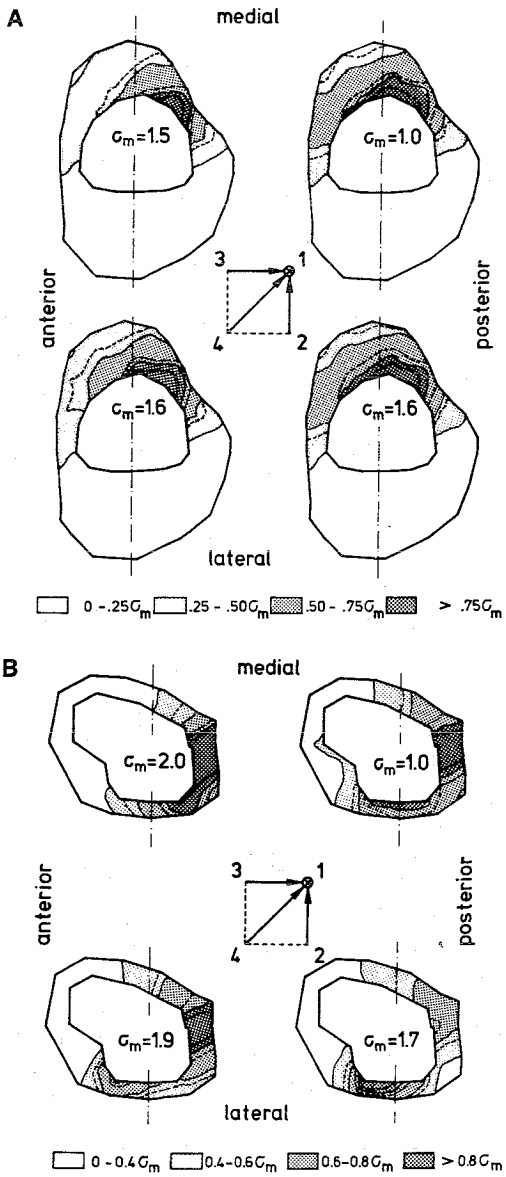

FIG. 24.6. Von Mises stress patterns in cancellous bone surrounding a short cementless prosthesis (10), in a proximal section **(a)** and a distal section **(b).** In case 1, the hip-joint force works in the (frontal) plane of symmetry of the prosthesis. In case 2, the force is rotated 15° laterally; in case 3, 15° anteriorly; and in case 4, 15° anterior/laterally. The stress values are shown relative to the maximal value σ_m occurring in each case in the section. The rotations of the force increase the maximal stresses about 50% on the proximal side and about 100% on the distal side.

such as CoCrMo alloys, have some distinct biomechanical advantages for the load transfer, in particular when acrylic cement is applied to compensate for the "elastic mismatch."

NUMERICAL BENCH TESTING

FEM models, with their limitations and schematic character, cannot always realistically predict precise stress values in particular patient cases, owing to the structural complexity and the variability in the *in vivo* configuration (3). However, they can be versatile tools to study particular general problems, evaluate specific effects, and analyze the biomechanical

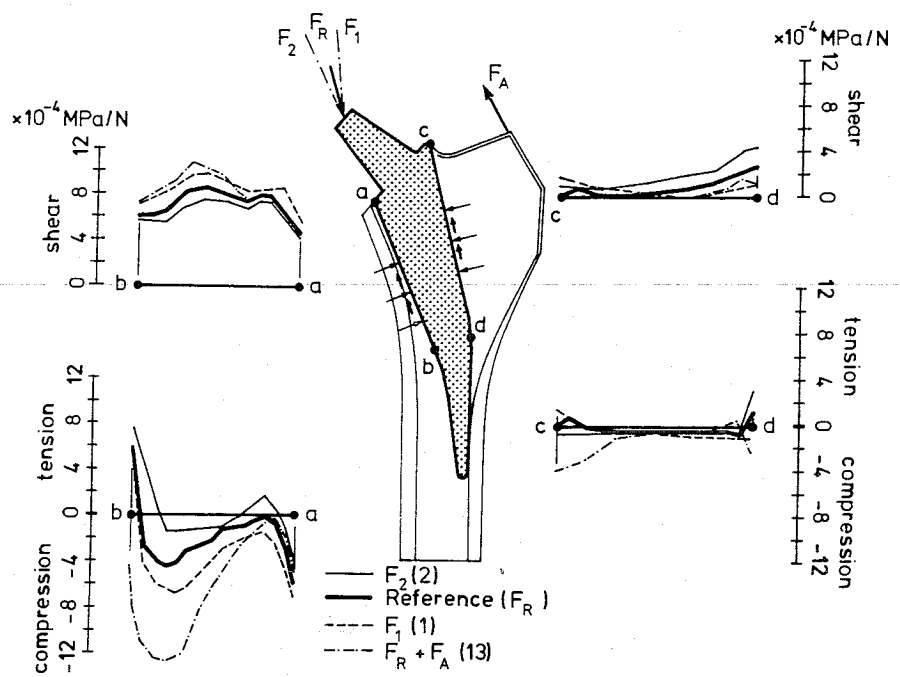

FIG. 24.7. Direct and shear stresses at the implant–bone interface, as determined for various loading characteristics (10). The stresses are high, in particular when the load causes a high bending moment.

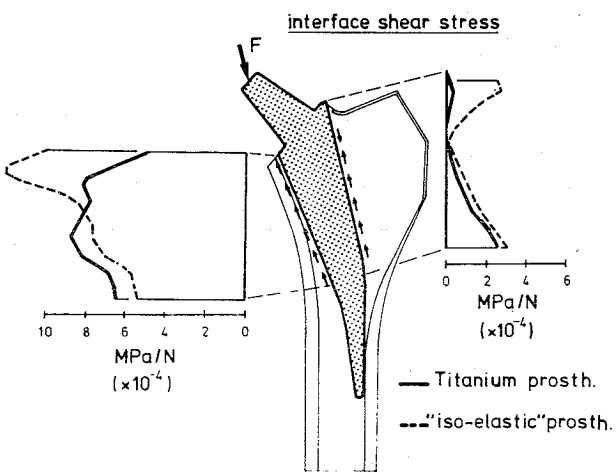

FIG. 24.8. Shear stresses at the medial and lateral implant–bone interface, comparing titanium as stem material with a hypothetical isoelastic material with the same elastic modulus as cortical bone (10).

characteristics of implant designs on a comparative basis. The latter application is the objective in numerical bench testing. A problem in the comparison of joint designs for which FEM analyses have been reported is that the model characteristics, bone geometry and properties, and the loading are usually vastly different. This problem can be overcome by the use of standard models. The 2-D side-plate FEM model in Fig. 24.5 is used in our laboratory to test different stem designs on a relative basis in a standardized fashion (16). The bone geometry and properties are equal in all cases and based on earlier geometrical and strain-gauge analyses of bone specimens (14). Three subsequent loading cases are always included, a bending moment on the femoral head and two forces, one representing the one-legged stance (17) (F_1, Fig. 24.5) and one 10° rotated laterally (F_2, Fig. 24.5). Regardless of the prosthetic design, the loading configuration with respect to the bone geometry is always equal, and stress comparisons are made relative to corresponding nodal points. The placement of the stems is done in accordance with the manufacturer guidelines; hence, the concept of a design is tested rather than a particular patient case.

An example of stress comparisons relative to six (cemented) designs is shown in Fig. 24.9 [MSS: Müller Straight Stem; EXE: Exeter; MCS: Müller Curved Stem; SCH: Scandinavian Hip (experimental design); HMA: Howmedica Precision Hip]. Shown are (a) stress values at the medial cortex, 20 mm below the calcar, in comparison to natural; (b) maximal stem stresses; and (c) maximal stresses in the proximal and distal cement, representing load transfer in these areas in general. The bars represent the value ranges when the force is rotated from F_1 (always the lowest value) to F_2 (Fig. 24.5).

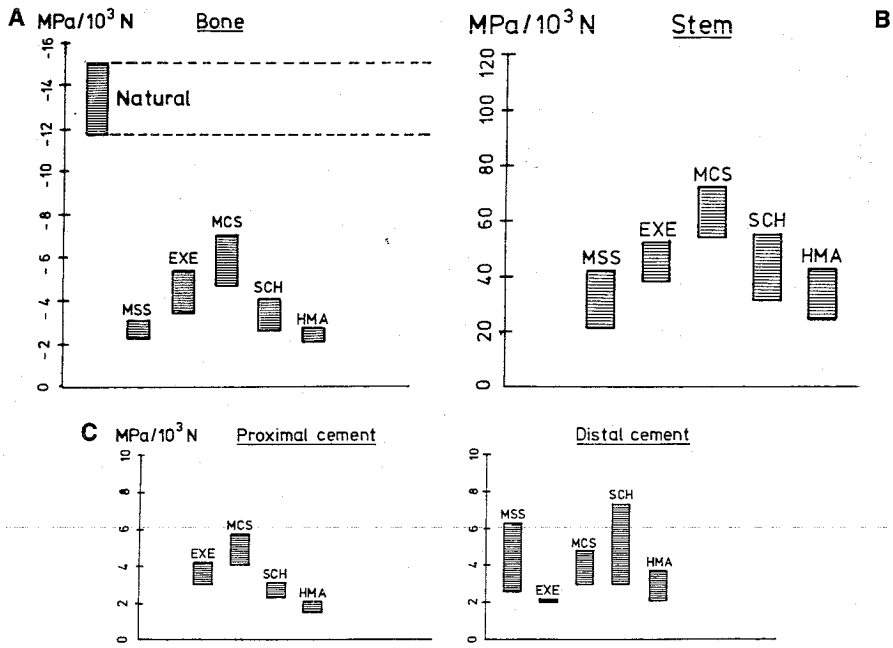

FIG. 24.9. A comparison of stress values associated with five different cemented prostheses (16). The lowest value of the bar is always for the force F_1 (compare Fig. 24.5); the highest value, for the 10° lateralized force F_2. **A:** Parallel (bending) stress at the periosteal bone surface 20 mm from the calcar. **B:** Maximal von Mises stress in the stem. **C:** Maximal von Mises stress in the proximal and distal cement (there is no proximal/medial cement in the MSS design).

It is evident from these results that design selections relative to alternative biomechanical criteria such as stress-shielding, maximal stem stresses, and cement–interface stresses are a matter of compromising. Apart from applications to design selection and design adaptations, these load-transfer characterizations are helpful in clinical research, to enhance roentgenological observations.

The FEM model used in this case is relatively simple, only because 3-D models would, at this point in time, be too expensive and time consuming for the purpose of the test. However, it is likely that in the future, while computer capabilities are rapidly increasing, standardized 3-D FEM models will be developed for comparative testing of commercial implant designs.

NUMERICAL DESIGN OPTIMIZATION

FEM results, as described in the previous section, can be used for a process of stem-design optimization, by adapting geometrical characteristics based on the stress results. Traditionally, this process of computer aided design is one of trial and error, based on the creativity of the designer, guided by the FEM results, possibly in combination with systematic parametric variations in subsequent calculations. Because the number of possible combinations of structural variations in a prosthetic design, even a simple femoral stem is quite extensive, neither of these methods guarantees a truly optimal design.

Recent advances in computer methods, however, enable the application of direct numerical optimization, whereby FEM-integrated optimization codes determine the optimal shape for some arbitrary optimization criterion, based on an initial geometry (18). Schematically, this process is illustrated in Fig. 24.10. Two aspects of this scheme must be explained first. In all cases, a design criterion must be selected, such as minimal cement stresses,

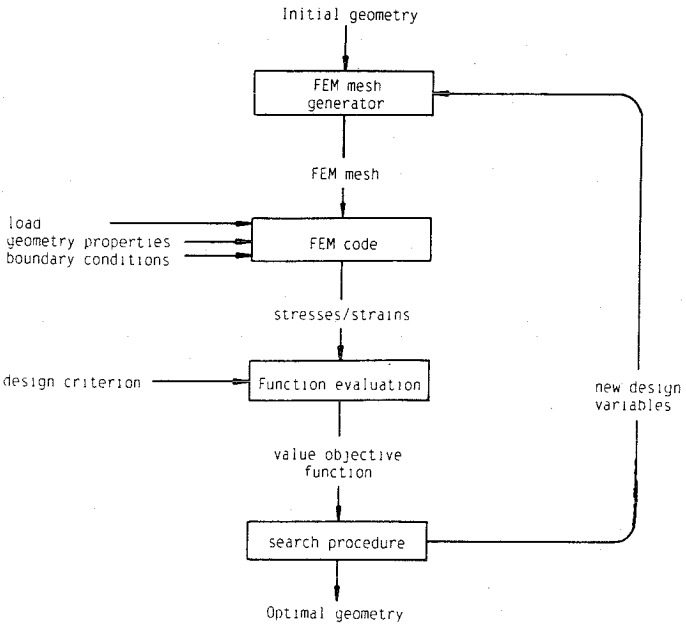

FIG. 24.10. Schematic representation of the numerical optimization scheme (18).

minimal implant–bone interface stresses, or any other criterion, based on an expectation about the most important failure mode. This criterion must be mathematically described in an objective function, which becomes the subject of a minimization procedure. The second aspect concerns the representation of the geometry of the design, which must be described with a finite number of design variables, e.g., the stem length or the thickness at a number of locations along the stem. The higher the number of design variables, the more computer-time-consuming the process becomes.

The core of the code is the normal FEM program, including mesh generation, the first two blocks in Fig. 24.10. From the FEM results, the value of the objective function for the actual values of the design variables is determined. In a search procedure, which involves iterative loops through the FEM code, the design-variable values, for which the objective function is minimal, representing the optimal shape, are determined.

An example (18) of such an FEM optimization procedure is shown in Fig. 24.11, involving the simple model of Fig. 24.3, whereby the stem is loaded with an axial force. The design criterion used is based on minimal cement–bone interface shear stresses. The bone

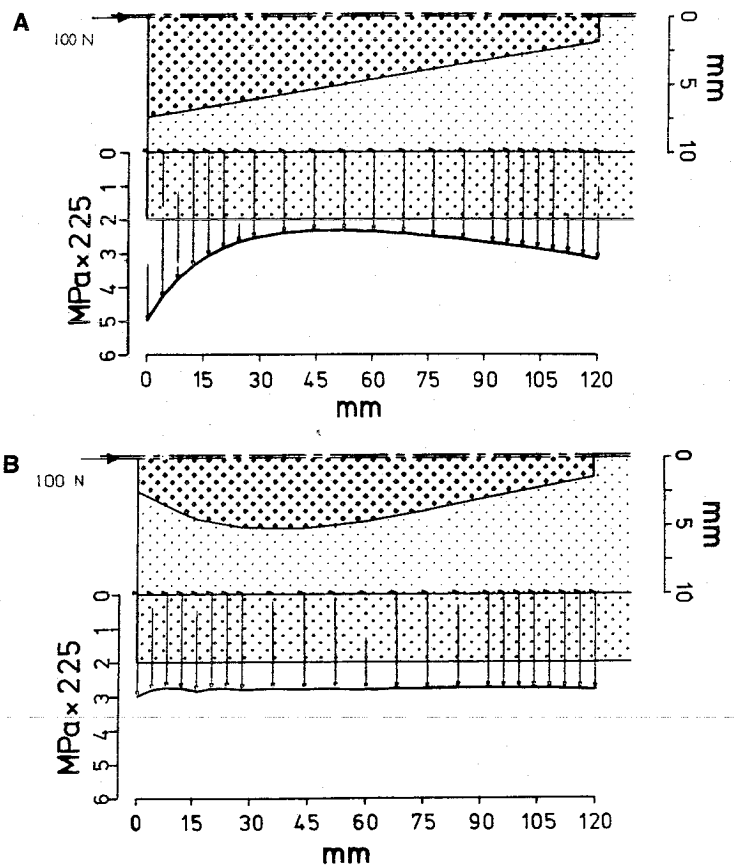

FIG. 24.11. Cement–bone interface shear–stress patterns in a simplified intramedullary fixation model, under axial loading (compare Fig. 24.3). Both stem shapes are numerically optimized with the objective of minimal interface shear stresses. In one case **(a)** the stem contour is described by two design variables (proximal and distal diameters); in the other case **(b)**, nine design variables are used (stem diameters at nine locations along the stem).

geometry and all material properties are fixed. The stem length is preset at 120 mm. Shown are the resulting shear–stress patterns for two optimal configurations: (a) whereby the stem geometry is described by two design variables, the stem thickness at the medial and proximal ends (hence, a straight taper), and (b) whereby the stem thickness is described by nine design variables, the stem thickness at nine locations along the stem.

In the case of a straight stem (Fig. 24.3), stress peaks occur at the proximal and distal interfaces. In the case of a straight taper (Fig. 24.11), the distal stress peak in particular is reduced. Because the shear stresses at the interface must balance the applied load of 100 N, the minimal shear stress feasible would be a uniform one, with the magnitude of load divided by total interface area, which in this case is 1.33×10^{-2} MPa. As shown in Fig. 24.11, the stem shape for which this optimal stress distribution is realized can indeed be found with the FEM optimization procedure, provided that the number of design variables selected (nine in this case) is adequate. It is interesting to note the cigar-like shape of this optimal stem.

It must be borne in mind that this is only a simple example, meant to illustrate the procedure. In a more realistic model, optimal shapes can be determined in basically the same way, whereby stress reductions can be as high as 60% (18).

Two aspects are of importance when working with these numerical tools. One is that the actual application of optimal designs is subject to practical limitations. For instance, there is a natural variation in bone geometry and a limit to the surgical accuracy obtainable. Second, the optimal shape depends on the objective function and therefore on the design criterion selected. Hence, even more so than with the traditional, creativity-driven method, it is imperative that definite knowledge about the most significant clinical failure modes is available.

PRIMARY AND SECONDARY "STABILITY"

The previously discussed numerical tests and optimization methods are usually carried out with FEM models describing an idealized configuration, based on the concept of a THA structure in the immediate postoperative situation, whereby stress patterns are interpreted regarding their chances to initiate mechanical failure. Although this certainly seems a worthwhile endeavor, two complicating aspects reduce its usefulness. One is that bone, being a biological tissue, changes its structure over time. The second is that, as already discussed in the introduction, a mechanical failure may be the onset of clinical failure, but these phenomena are certainly not synonymous, and a THA with a mechanical failure (e.g., a loosened cement–stem or implant–bone interface) may still function clinically for a long period of time. Both the biological adaptations and the mechanical failures result in altered stress patterns, to which the original, idealized FEM predictions no longer apply.

An example illustrating changes of this kind is in Fig. 24.4, in which the implant–bone interface shear–stress patterns for the MSS and EXE prostheses are also presented for the case that 20 mm calcar resorption would have occurred. Evidently, the effect of such a phenomenon depends on the design of the prosthesis: whereas the proximal shear–stress peak associated with the stiff MSS stem merely shifts distally, the peak associated with the flexible EXE stem almost doubles in value.

Hence, the design of a prosthesis not only determines the chances of mechanical failure to be initiated, but also the chances of failures to rapidly propagate. To separate these two mechanical capacities, we have suggested (19) the terms *primary stability* for the

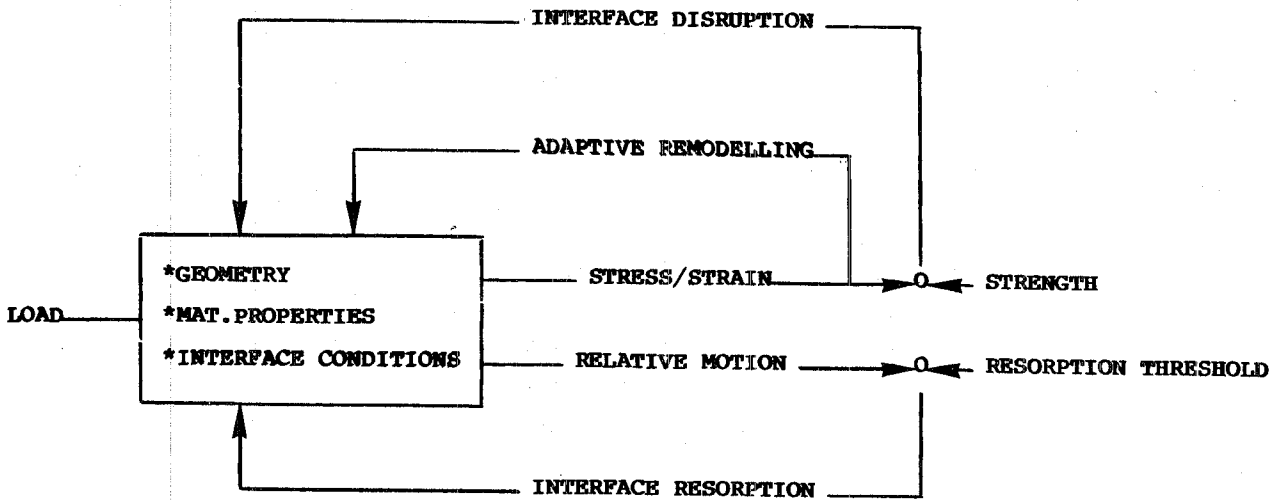

FIG. 24.12. Schematic representation of mechanical phenomena involved with the processes of bone remodeling and joint loosening.

potential of a joint design to withstand primary mechanical failure of any kind in the immediate postoperative situation versus *secondary stability* for its potential to withstand rapid mechanical deterioration after mechanical failure or biological adaptions have occurred. For example, according to this definition and Fig. 24.4, the EXE prosthesis would have a better primary stability and the MSS design a better secondary stability.

The question of primary stability, which is related to the hypothetical stochastic model of Fig. 24.2, is actually addressed by FEM analyses, as discussed in the previous sections. The matter of secondary stability, however, is much more complicated, because it involves multifactorial failure modes and biological/mechanical interactions that are not well understood and are difficult to analyze. An example of the former is stem–cement interface loosening, which is probably very common (20) and has a drastic effect on cement and cement–bone interface stresses (21). Other examples are cement cracks (22,23) and implant–bone failure propagation (24). Examples of biological changes are cortical osteopenia caused by stress shielding (25) and micromotion-induced interface resorption and soft-tissue interposition (26).

The secondary stability of an implant design is possibly even of higher clinical relevance than primary stability. In analyzing the histomorphology and biomechanics of failed surface replacements (19), it was found that, when compared with other kinds of implants, the high failure rates of this prosthesis could be explained by an inferior secondary stability, rather than by an inferior primary stability. In the failure process, micromotion-induced interface resorption in particular appeared to have played a role. Other investigators came to the same conclusion after analyzing failed THA (27,28).

Assuming that stress-shielding effects cause adaptive remodeling, and that interface bone resorption is controlled by relative (micro) motions between implant and bone, the scheme in Fig. 24.12 describes conceptually the most important mechanical phenomena determining primary and secondary stability of an implant. Traditional FEM analysis, addressing the primary stability only, is limited to the idealized initial structure, whereby one set of stress–strain patterns is determined, based on one or more particular loads. The objective of FEM development in this field, at least in our laboratory, is to enable analyses of the whole cycle, including the feedback loops. Although much development and experimentation are still to be done before this stage is reached, two aspects of recent developments are illustrated in the next sections. The first concerns the consequences of cement–bone interface loosening and fibrous-tissue interposition on the load-transfer mechanism and the stress patterns; the second concerns the effects of stress shielding on cortical osteopenia.

INTERFACE LOOSENING AND BONE RESORPTION

The mechanical behavior of a fibrous-tissue interface layer is governed by the following effects (29): (a) a reduced compliance, relative to bone, (b) material nonlinearity in compression (Fig. 24.13), (c) very little resistance against tension (tensile separation), (d) slip in shear, and (e) time dependency (viscoelasticity). The presence of such a layer in knee arthroplasty was shown to affect interface stress patterns (30,31). Where the femoral THA is concerned, Brown et al. (32) reported some effects on the stress patterns, based on a 3-D FEM analysis. However, in this model (32) the layer was considered as a linear elastic material, rigidly bonded on two sides to the cement and the bone. Hence, only the first of these effects was taken into account. Using nonlinear FEM analysis, whereby effects (a) through (d) are adequately described, it can be shown that the linear approximation is inadequate (33).

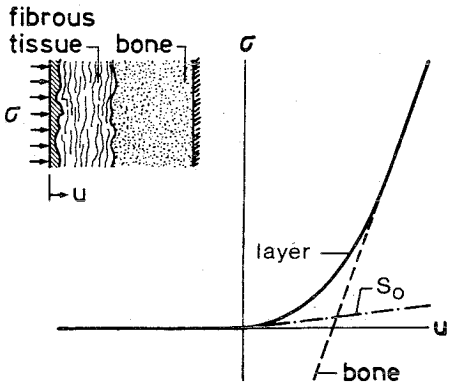

FIG. 24.13. Approximate description of stress-displacement characteristics of the fibrous-tissue interface layer (33). The initial stiffness (S_0) is small but progressively increases to infinity when the layer is pushed through; in that case, the interface stiffness is again governed by the bone.

Figure 24.14 shows some examples (33) of stress patterns in bone and prosthesis, determined in a 2-D side-plate model, comparable to the one in Fig. 24.5, using the nonlinear FEM. The different graphs represent the stress patterns for (I) a bonded interface (the normal linear case); (II) a bonded, linear elastic interface layer of 1 mm, with a reduced, 10 MPa elastic modulus [similar to the analysis of Brown et al. (32)]; (III) an interface layer as in the previous case, but this time allowing slip and tensile loosening; and (IV)

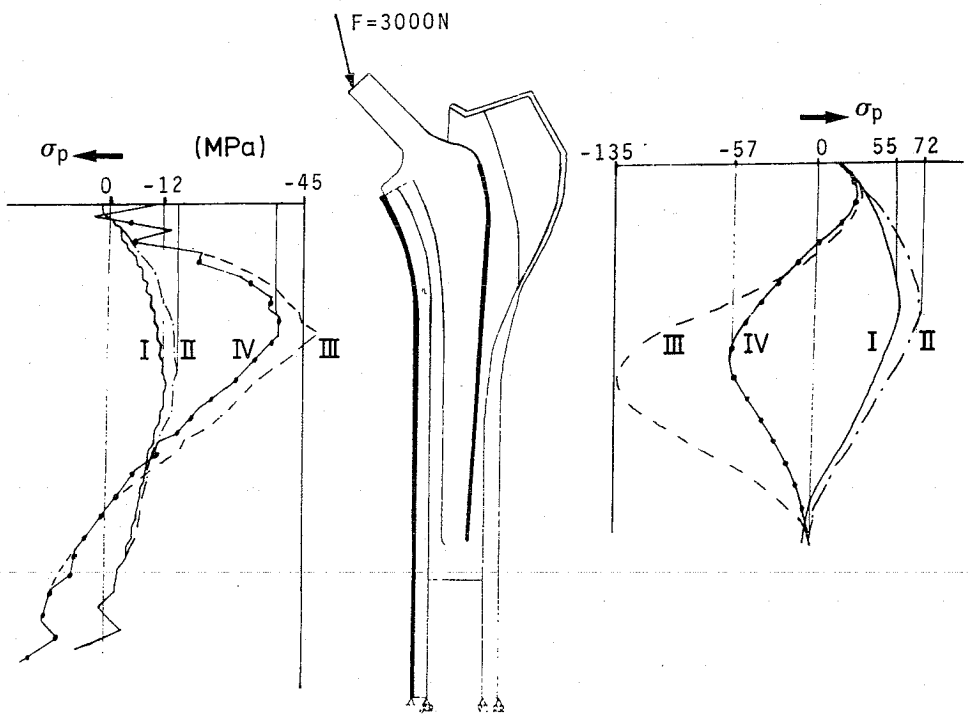

FIG. 24.14. Parallel (bending) stresses along the medial periosteal surface **(left)** and along the lateral stem surface **(right),** comparing four models (33): I: Normal bone bond at the cement–bone interface. II: Linear elastic soft (10 MPa) layer of 1 mm, bonded to the cement and the bone. III: The same as II, but unbonded (tensile separation and slip). IV: The same as III, but with nonlinear elastic compressive properties (compare Fig. 24.13).

loosening conditions as in the previous case, with an interface layer also of 1 mm thickness, with nonlinear elastic properties (as in Fig. 24.13).

As illustrated in Fig. 24.14, the linear fibrous-tissue interface model (II) results in increased bone and stem (bending) stresses, compared with the model with a normal bone interface (I). However, very dramatic effects on the load-transfer mechanism and the stress patterns are predicted when the tensile loosening and slip effects are realistically accounted for (model III). The additional aspect of nonlinear elastic properties of the fibrous-tissue layer (IV) change the stress patterns, relative to model III, only in a gradual sense; the trends of the models III and IV are similar.

Figure 24.15 shows stem–cement interface stresses, comparing the case of the normal, bonded bone interface (I) with the case of an unbonded, nonlinear fibrous-tissue layer (IV). It must be noted here that the collar is not in contact with the calcar. A dramatic increase of interface stresses (compression) is evident, concentrated at the medial/proximal and the middle/lateral sides. The prosthesis, surrounded by a fibrous-tissue layer, has lost its normal close-fit support and is pushing through the layer, finding new support in two regions only, thereby almost loaded in three-point bending.

These findings illustrate that bone necrosis and fibrous-tissue formation at the implant–bone interface have dramatic effects on the load-transfer mechanism. These effects are caused mainly by the tensile loosening/slip characteristics of the interface, in combination with the low compliance of the fibrous-tissue layer, the effects (a), (c), and (d). The additional effect of nonlinear elastic behavior in compression (b) is notable but not as pronounced as the others.

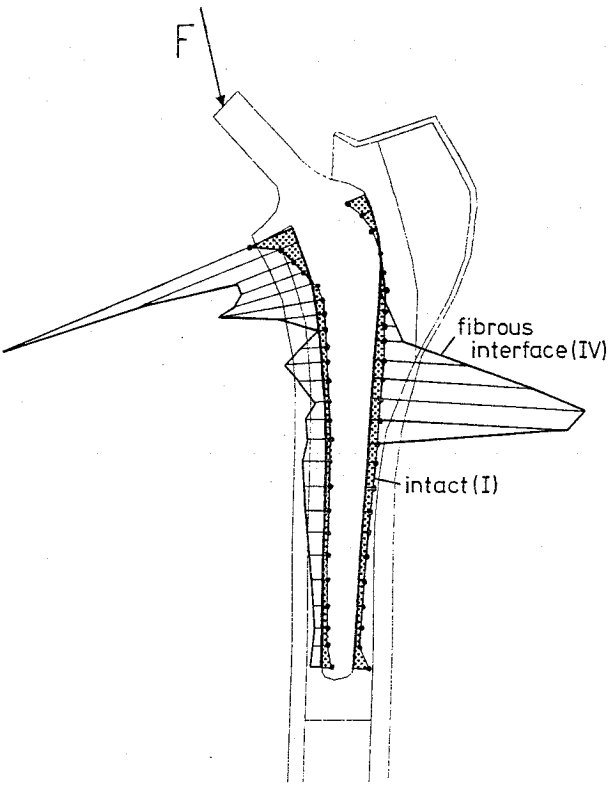

FIG. 24.15. Normal, direct stresses at the stem–cement interface (outside the stem surface compression, inside tension), comparing the effects of a normal bone-bonded cement–bone interface (I) to those of a (nonlinear) fibrous-tissue interface layer of 1 mm (IV) (33).

The precise effects of the prosthetic behavior in the fibrous-tissue layer, how it subsides and where it finds support, depend highly on the 3-D shape of the implant–bone interface contour and on the thickness variation of the layer. Hence, relative to the clinical reality, the above results can only describe trends. These trends, however, indicate that the stress patterns in the THA structure change dramatically in the process of interface loosening and that the loosening propagation scheme suggested in Fig. 24.12 is a realistic one.

STRESS SHIELDING AND CORTICAL OSTEOPENIA

The second feedback loop in Fig. 24.12 concerns the relation between bone stress and adaptive remodeling. Although it is widely assumed that stress shielding, as discussed in the second section relative to Fig. 24.3, causes disuse osteoporosis or osteopenia, very little is known about the actual mechanism of this relation. Research in this area started late in the last century with Meyer, Culmann, Wolff, and Roux and is carried on until the present day (34). Clinical evidence of osteopenia associated with implants has been reported in relation with bone plates and intramedullary prostheses (25,35–40). Based on the assumed relation with stress shielding, these findings are usually associated with rigid implants or bone ingrowth, whereby it must be noted that bone-ingrowth prostheses are usually relatively rigid as well.

The mechanical consequences of adaptive bone remodeling in THA can be analyzed with FEM codes, in combination with mathematical descriptions of the adaptive process, in the sense of the feedback loop in the scheme of Fig. 24.12. An example of such a simulation model (41) is described in Fig. 24.16. This model is based on the theory of adaptive elasticity (42) and a number of hypothetical assumptions. For the control signal of the adaptive process, the "strain energy density" U (MPa) is selected. The local values of this variable in bone are determined in the FEM model and compared to the predetermined "natural" values U_n. A discrepancy leads to addition or subtraction of bone mass in either of two ways. One is internal remodeling (e.g., osteoporosis), which causes a change of bone density and hence of elastic modulus; the other is external, or surface, remodeling, which results in a change in bone shape (e.g., cortical thinning). The adaptions in elastic moduli or bone geometry are effected in the FEM model, and a new iteration starts. This process continues until a stable configuration is reached, whereby the strain energy density is normalized within certain limits, or until all bone has disappeared.

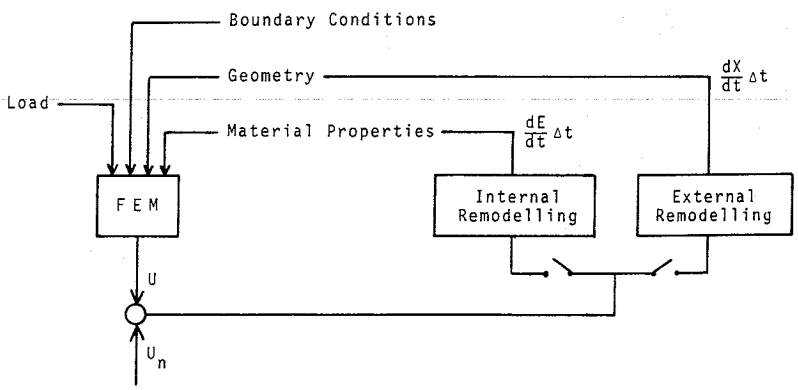

FIG. 24.16. Scheme of the FEM-integrated, adaptive bone remodeling program (41).

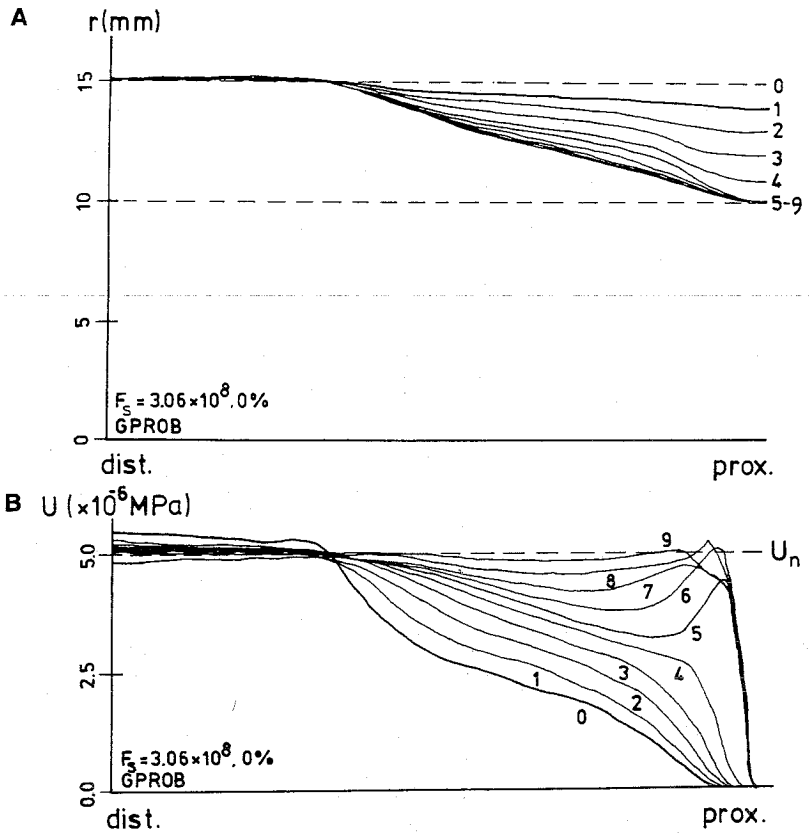

FIG. 24.17. **A:** Development of the outer-bone radius after subsequent remodeling iterations 1–9. **B:** Development of the strain energy density at the bone surface, after subsequent remodeling iterations 1–9.

An example (41) involving again the simplified model of Fig. 24.3 (straight stem, straight bone), loaded in bending, is shown in Fig. 24.17. In the intact, immediate postoperative configuration (iteration 0), the bone is straight (uniform outer radius R_o = 15 mm) and the periosteal strain energy density U is considerably reduced relative to the natural value U_n, in particular at the proximal side, owing to stress shielding (compare with Fig. 24.3). In subsequent iterative steps (1–9), bone is removed from the surface, whereby the strain energy density increases toward the natural value U_n.

In this example, the stem has a diameter of 13.3 mm. The final configuration, relative to the initial one, is again shown in Fig. 24.18, together with final configurations determined for stems of 10 and 20 mm diameter. The amount of bone removal associated with the 10 mm stem is smaller in comparison. The rigid, canal-filling 20 mm stem causes the bone adjacent to the stem to disappear almost completely. In other words, the amount of stress shielding is so high, as a result of the stem rigidity, that the bone is unable to reach a natural strain state.

Evidently, these results are highly hypothetical, owing to the simplicity of the FEM model and the assumed relation between strain-energy density and adaptive remodeling. However, they do illustrate contemporary capabilities of FEM analysis. These simulation

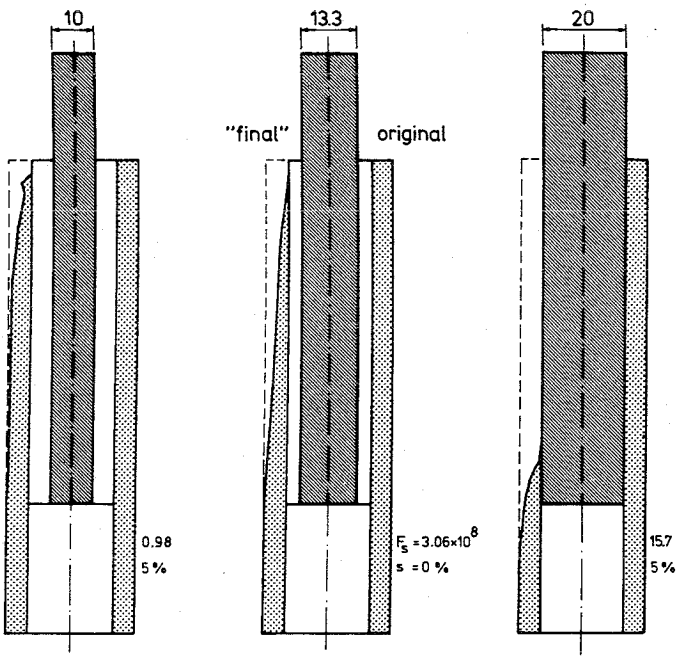

FIG. 24.18. Final configurations of the remodeled bone, determined for three stem diameters (41).

models can be very helpful, when used in combination with animal or clinical experiments, to improve our knowledge about the adaptation process around prostheses and its consequences for the postoperative changes in the load-transfer mechanism.

DISCUSSION

It can be concluded from this brief overview that the general load-transfer mechanism and the associated stress patterns in the mechanically intact femoral THA are well documented by FEM and experimental analyses. Most work has been done relative to cemented designs, but there is in principle no limitation to the application of the same methods for (bonded) cementless prostheses. Applications of accurate 3-D FEM analyses are still limited by present computer capacities and 3-D graphics feasibilities, but these are rapidly improving. The absolute validity of FEM predictions could certainly improve with more precise knowledge about physiological hip-joint loading characteristics, also in functions other than walking or stair climbing. Another improvement in this respect could be found in more accurate descriptions of bone elastic properties, in particular where nonuniform density distributions and anisotropy of trabecular bone are concerned.

Comparisons on a relative basis show that the actual stress patterns associated with various prosthetic designs can be distinctly different. Because these stress patterns are highly susceptible to model characteristics and the hip-joint load, the use of standardized FEM models to compare the performance of commercial designs seems worthwhile. Such a process of numerical bench testing is relatively simple with present-day 2-D FEM models. The application of 3-D models for this purpose will certainly become equally feasible in the near future.

These analyses all concern the primary stability of the implant, whereby the central question is whether a particular design is likely to fail mechanically in any way. Because of the variability in patient parameters, surgical technique, and actual functional loading, the FEM models are by necessity representative of a schematic, generalized reality. Hence, the above question is difficult to answer in an absolute sense. Of course, a prosthetic design should be such as to cause minimal stem, cement, and interface stresses, and bone stresses should be as natural as possible. The problem, however, is that these objectives cannot all be realized to the same extent at the same time. Hence, information is needed about the relative importance of these different aspects. This is the more important when numerical optimization techniques are used, because in that case the design criterion must be predetermined as an objective function to be minimized. Our present feeling, based on our own research and on data in the literature, is that implant–bone interface stresses should be minimized, with some additional restrictions on stem and bone stresses, whereby cement stresses (in the case of a cemented prosthesis) will automatically be reduced as well. However, this is certainly not fully documented and requires further clinical and experimental research. The interpretation of the clinical significance of FEM results is still the most difficult aspect.

Developments in FEM techniques have simplified the analysis of nonlinear phenomena such as interface loosening and the effects of fibrous-tissue formation and bone remodeling. As a consequence of this, THA structures can be analyzed also relative to their gradual postoperative development, and the secondary stability of an implant design can be investigated. Initial studies in this direction have shown that the load-transfer mechanism and the associated stress patterns change tremendously during a loosening or bone remodeling phase. To further develop these applications in a way that they become clinically useful requires a correlation with bone and interface biology and with clinical-failure modes.

ACKNOWLEDGMENTS

The author wishes to acknowledge the assistance of the Biomedical Engineering group of the University of Twente, the financial support of the Netherlands Organization for the Advancement of Pure Research, and Grants from Orthopaedic Technology B.V., The Netherlands, and Howmedica Inc., New Jersey, for various aspects of the research work described in this chapter.

REFERENCES

1. Zienkiewicz OC. *The finite element method.* 3rd Ed. London: McGraw-Hill, 1977.
2. Huiskes R. Principles and methods of solid biomechanics. In: Ducheyne P, Hastings G, eds. *Functional behavior of orthopaedic materials. Vol. I: Fundamentals.* Boca Raton: CRC-Press, 1984:51.
3. Huiskes R, Chao EYS. A survey of finite element methods in orthopaedic biomechanics. *J Biomech* 1983;16:385.
4. Huiskes R. Some fundamental aspects of human-joint replacement. *Acta Orthop Scand (Suppl)* 1980;185.
5. Crowninshield RD, Brand RA, Johnson RC, Milroy JC. An analysis of femoral component stem design in total hip arthroplasty. *J Bone Joint Surg* 1980;62A:68.
6. Rohlmann A, Moessner U, Bergmann G, Koelbel R. Finite element analysis and experimental investigation in a femur with hip endoprosthesis. *J Biomech* 1983;16:727.
7. Lewis JL, Kramer GM, Wixson RL, Askew MJ. Calcar loading by titanium total hip stems. Chicago: *Proceedings 27th annual meeting Orthopaedic Research Society;* 1981:75.
8. Tarr RR, Clarke IC, Gruen TA, Sarmiento A. Predictions of cement-bone failure criteria. In: Gallagher RH, Simon BR, Johnson PC, Gross JF. *Finite elements in Biomechanics.* New York: John Wiley, 1982:345.
9. Vichnin HH, Batterman SC. Stress analysis and failure prediction in the proximal femur before and after total hip replacement. *J Biomech Eng* 1986;108:33.

10. Huiskes R, Snijders H, Vroemen W, Chao EY, Morrey BF. Fixation stability of a short cementless hip prosthesis. Proceedings 32nd Annual Meeting Orthopaedic Research Society, Chicago, 1986:466.
11. Jacob HAC, Huggler AH. An investigation into biomechanical causes of prosthesis stem loosening within the proximal end of the human femur. *J Biomech* 1980;13:159.
12. Oh I, Harris WH. Proximal strain distribution in the loaded femur. *J Bone Joint Surg* 1978;60A:75.
13. Crowninshield RD, Pedersen DR, Brand RA. A measurement of proximal femur strain with total hip arthroplasty. *J Biomech Eng* 1980;102:230.
14. Huiskes R, Janssen JD, Slooff TJ. A detailed comparison of experimental and theoretical stress-analyses of a human femur. In: Cowin SC, ed. *Mechanical properties of bone*—AMD Vol. 45. New York: The American Society of Mechanical Engineers, 1981:211.
15. Huiskes R. Biomechanics of bone–implant interactions. In: Schmid-Schönbein GW, Woo SL-Y, Zweifach BW, eds. *Frontiers in biomechanics*. New York, Berlin, Heidelberg, Tokyo: Springer-Verlag, 1986:245.
16. Huiskes R, Vroemen W. A standardized finite element model for routine comparative evaluations of femoral hip prostheses. *Orthop Trans* 9, 1985;2:254.
17. Crowninshield RD, Johnston RC, Andrews JG. A biomechanical investigation of the human hip. *J Biomech* 1978;11:75.
18. Huiskes R, Boeklagen R. Mathematical optimization of hip-prosthesis design. *J Biomech* (submitted).
19. Huiskes R, Strens P, Vroemen W, Slooff TJ. "Secondary stability" and relative motions in femoral resurfacing prostheses. *J Orthop Res* (submitted).
20. Huiskes R. Properties of the stem–cement interface and artificial hip joint failure. In: Lewis JL, Galante JO, eds. *The bone–implant interface*. Chicago: American Society of Orthopaedic Surgeons, 1985:86.
21. Hampton SJ. A nonlinear finite element model of adhesive bond failure and application to total hip joint replacement analysis. Ph.D. Thesis, University of Illinois, Chicago, 1981.
22. Gruen TA, McNeice GM, Amstutz HC. Modes of failure of cemented stem-type femoral components. *Clin Orthop Rel Res* 1979;141:17.
23. Stauffer RN: Ten-year follow-up study of total hip replacement. *J Bone Joint Surg* 1982;64A:983.
24. Lewis JL. Mechanical processes in bone–cement interface failure. In: Lewis JL, Galante JO, eds. *The bone-implant interface*. Chicago: American Society of Orthopaedic Surgeons, 1985:34.
25. Engh CA, Bobyn JD, Glossmann AH. Porous-coated hip replacement: the factors governing bone ingrowth, stress shielding, and clinical results. *J Bone Joint Surg* 1987;69B:45.
26. Perren SM, Ganz R, Rüter A. Über oberflächigen Knochenresorption und Implantat. *Med Orthop Transact* 1975;95:6.
27. Radin EL, Rubin CT, Thrasher BL, et al. Changes in the bone–cement interface after total hip replacement. *J Bone Joint Surg* 1982;64A:1188.
28. Eftekar NS, Doty SB, Johnston AD, Parisien MV. Prosthetic synovitis. In: Fitzgerald RH, ed. *The hip*. St. Louis: The C. V. Mosby Company, 1985:169.
29. Hori RY, Lewis JL. Mechanical properties of the fibrous tissue found at the bone–cement interface following total joint replacement. *J Biomed Mater Res* 1982;16:911.
30. Hori RY, Lewis JL, Hammer RS, Askew MJ. The effect of a fibrous tissue liner between bone and cement on finite element models of bone–prosthesis structures. *Proceedings 28th annual meeting Orthopaedic Research Society*, Chicago, 1982:146.
31. Vanderby R, Lewis JL, Chapman SM. Biphasic modeling of fibrous tissue at the bone–prosthesis interface in total joints. In: Langrana NA. *1985 Advances in Bioengineering*. New York: The American Society of Mechanical Engineers, 1985:22
32. Brown TD, Pedersen DR, Radin EL, Rose RM. Global mechanical consequences of bone/cement interface degradation in proximal femoral arthroplasty. *Proceedings 32nd annual meeting Orthopaedic Research Society*, Chicago, 1986:467.
33. Weinans H, Huiskes R, Grootenboer H. The modelling and mechanical consequences of fibrous-tissue formation around femoral hip prostheses. In: Butler DL, Torzilli PA, eds. *1987 Biomechanics Symposium*. AMD-Vol. 84. New York: American Society of Mechanical Engineers 1987:89.
34. Currey J. *The mechanical adaptations of bone*. Guildford, U.K.: Princeton University Press, 1984.
35. Tonino AJ, Davidson CL, Klopper PJ, Linclan LA. Protection from stress in bone and its effects. *J Bone Joint Surg* 1976;58B:107.
36. Pilliar RM, Cameron HU, Szivek J, Binnington AG, MacNab I. Bone ingrowth and stress shielding with a porous surface coated fracture fixation plate. *J Biomed Mater Res* 1976;13:799.
37. Miller JE, Kelebay LC: Bone ingrowth—disuse osteoporosis. *Orthop Trans* 1981;5:380.
38. Engh CA, Bobyn JD. *Biological fixation in total hip arthroplasty*. Thorofare, New York: Slack Inc., 1985.
39. Brown IW, Ring PA. Osteolytic changes in the upper femoral shaft following porous-coated hip replacement. *J Bone Joint Surg* 1985;67B:218.
40. Turner TM, Sumner DR, Urban RM, Rivero DP, Galante JO. A comparative study of porous coatings in a weight-bearing total hip-arthroplasty model. *J Bone Joint Surg* 1986;68A:1396.
41. Huiskes R, Weinans H, Grootenboer HJ, Dalstra M, Fudala B, Slooff TJ. Adaptive bone-remodelling theory applied to prosthetic-design analysis. *J Biomech* 1987;20:1135–1151.
42. Cowin SC, Hegedus DH. Bone remodelling I: Theory of adaptive elasticity. *J Elasticity* 1976;6:313.